

## Three-body correlations in the amorphous $\text{Ni}_{80}\text{B}_{20}$ and $\text{Fe}_{90}\text{Zr}_{10}$ alloys probed by x-ray-absorption near-edge structure calculations

Peter Kizler

*Hamburger Synchrotronstrahlungslabor (HASYLAB) at Deutsches Elektronen-Synchrotron DESY,  
Notkestrasse 85, D-22603 Hamburg, Germany*

(Received 17 June 1992; revised manuscript received 8 June 1993)

X-ray-absorption near-edge structure (XANES) data have since long been expected to provide information on third- (or higher-) order correlations in materials. In the present study, three-body correlations in amorphous alloys are studied by taking advantage of XANES data. The detailed analysis of XANES results computed for amorphous alloys of the  $\text{Ni}_{80}\text{B}_{20}$  and the  $\text{Fe}_{90}\text{Zr}_{10}$  type provide evidence that a fraction of the atoms in the structure are likely to contribute more to the final shape of the XANES result than the other atoms. In this connection, significant contributions of electron multiple-scattering processes are responsible for the shapes. In pursuit of a structural property to link short-range geometry and multiple scattering, together with significant contrast related to the different XANES shapes, atomic triangles of defined size are introduced as a criterion to interpret XANES results. An approach introduced to display graphically the abundance of such triangles serves as a basis for further discussions. In the case of  $\text{Ni}_{80}\text{B}_{20}$ , the XANES results threw light on metal-metal-boron triangles with certain measures, which are likely to be of particular interest in the structure. These triangles are characterized by one metal-boron distance between 0.19 and 0.21 nm and to a smaller fraction between 0.26 and 0.29 nm, whereas the triangles' other two sides are of average value within the ranges of the peaks of the partial pair-correlation functions. For the Zr neighborhood in  $\text{Fe}_{90}\text{Zr}_{10}$  it turned out that triangles with measures deviating from average values should occur less numerously than in the discussed model.

### I. INTRODUCTION

Techniques for determining atomic arrangements such as diffraction or extended x-ray-absorption fine-structure (EXAFS) spectroscopy usually give only the pair-correlation functions of the system. They describe the deviation of the atomic density of  $j$  atoms around  $i$  atoms from the average density of the material.

In the case of crystalline materials with their full lattice structure, all higher-order correlations (like bond angles) are implied and do not provide any additional information about the structure. In the case of disordered solids or liquids, the terms for pair and higher-order correlations, however, are partly decoupled, and knowledge of the latter promises valuable additional information about the structure of the material.<sup>1,2</sup> Yet pair and higher-order correlations can never be completely independent, because the necessity to fill a given space densely with atoms restricts the choices of possible atomic arrangements. Due to the nature of the disordered or distorted structure, such higher-order correlations can probably not be attributed to one single structural element like a unit cell or to one coordination polyhedron that can be investigated in geometrical studies of structural models.<sup>3</sup> Instead, a statistical description of the abundance of structural features has to be expected.

Besides bond-angle determination from field-ion microscopy (FIM) measurements<sup>4</sup> with their limited accuracy, a promising method to study many-body correlations was made available by numerical simulations of x-ray-

absorption near-edge structure (XANES) data.<sup>5</sup> Within roughly 50 eV beyond the absorption edge, the electrons emitted by the x-ray absorbing atom are able to perform multiple-scattering (MS) events, thereby interacting with more than two atoms. Durham, Vvedensky, and co-workers provided powerful computer algorithms to numerically calculate XANES data starting from structural data.<sup>5,6,7</sup> One of the advantages of Vvedensky's<sup>7</sup> code over the first version of Durham<sup>6</sup> is the option to suppress all MS processes, thereby to perform a curved wave single-scattering calculation (CWSS), equivalent to modern curved wave EXAFS calculation schemes. This feature of the code offers a chance to study in detail the contribution of MS to a XANES curve. The MS approach as a method to calculate local densities of states<sup>6</sup> is equivalent to the band-structure approach as an alternative interpretation for x-ray-absorption spectra.<sup>8</sup> Such calculations yield theoretical XANES spectra based on geometrical structures. Unlike for diffraction or EXAFS, in the XANES case there is no straightforward way to proceed from experimental data to structural information. Instead, XANES spectra have to be calculated from trial structures.

Depending on the agreement between calculated and experimental data, the trial structure can be estimated to be more or less realistic. MS calculations have already demonstrated the sensible connection between XANES results and bond angles in the trial structure,<sup>5,9</sup> on the ratio of distances of the x-ray absorbing atom to its first- and second-shell neighbors,<sup>9</sup> or on the perimeters of triangular scattering paths.<sup>10</sup>

## II. EARLIER XANES CALCULATIONS FOR AMORPHOUS ALLOYS

### A. $\text{Pd}_{80}\text{Ge}_{20}$

A first attempt to benefit from XANES calculations was to simulate Ge XANES spectra for some selected short-range clusters in amorphous  $\text{Pd}_{80}\text{Ge}_{20}$ .<sup>11</sup> However, in the true structure of an amorphous alloy, even if described by a structural model, there are not only ideal short-range polyhedra but also distorted, "frustrated" ones. They exist at the border between groups of nicely linked structural units, and second they can be caused by small positional movements of the atoms during energetic relaxation of the entire arrangement. Furthermore, the calculations of Ref. 11 were performed with only one shell of atoms around the x-ray absorbing atoms. As a common experience from other XANES studies, typically, a cluster with a radius of approximately 0.5 nm is required for a reliable calculation of XANES data, see e.g., Refs. 9 and 12.

### B. $\text{Ni}_{80}\text{B}_{20}$ (and $\text{Fe}_{80}\text{B}_{20}$ )

XANES calculations have to start from geometrical trial structures. For noncrystalline materials with a large variety of individual surroundings, this strategy seems hopeless but becomes practicable as soon as a structural model in Cartesian coordinates is available which takes into account structural information already available otherwise, essentially diffraction data. A random choice of central atoms out of such a model (hereafter termed "core atoms"), together with the clusters of atoms surrounding each of them within a radius of approx 0.5 nm must be selected, which then serve as input for the MS program. The XANES results for the whole model equals the average of all individual XANES results.

Following this strategy, XANES spectra of the Fe and Ni edge in amorphous  $\text{Fe}_{80}\text{B}_{20}$  and  $\text{Ni}_{81}\text{B}_{19}$  have been calculated<sup>13</sup> in good agreement with experimental data. The structures of the Fe and the Ni alloys were tentatively treated as identical, neglecting the small differences between the atomic distances.<sup>14,15</sup> This previous study made use of five different structural models set up for the alloys, whose partial pair-correlation functions agreed well with diffraction data.<sup>14,15</sup> In addition, these models were very similar with regard to angular correlation functions and statistical distribution of coordination numbers.<sup>16</sup> In this earlier study,<sup>13</sup> the calculations had been performed for a random choice of 40 core atoms out of each model. The exorbitant demand of computer time for the MS calculations restricts the allowed number of selected core atoms. [CPU time required for one individual XANES result out of the complex structure in Fig. 1 for one core atom: CRAY-XMP: (code is not highly vectorizable) ~ 10 min, VAX 9000: ~ 30 min, VAX 6000: ~ 2 h,  $\mu\text{VAX}$ : ~ 1.5 days. Any symmetry in the structure would speed up the calculation dramatically, but in the case of amorphous alloys there is no such property to take advantage of this.] The average of the 40 single calculations formed the XANES result (Fig. 1) for each

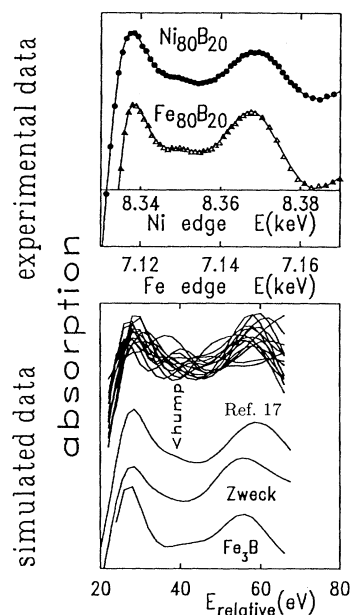


FIG. 1. Top part: experimental XANES data for the metal edges in amorphous  $\text{Ni}_{80}\text{B}_{20}$  and  $\text{Fe}_{80}\text{B}_{20}$  alloys. Lower part: random selection of individual XANES calculation results for the model of Dubois *et al.* (would look similar for any model). Lower curves: results for the models of Dubois *et al.* and Zweck obtained as the average of 322 or 380, respectively, (individual curves like the ones above). Bottom curve: calculated for  $\text{Fe}_3\text{B}$  (bct).

model. The essential difference among the results was how well the hump around 40 eV on the theoretical scale was reproduced by the calculations. MS calculations starting from the model of Dubois, Gaskell, and Le Caër,<sup>17</sup> followed by calculations from the model of Zweck,<sup>18</sup> agreed best with the experimental data, but even for these models the hump reproduced is not quite as satisfactory as desired.

More elaborate calculations had been performed, removing either the MS part altogether (see Ref. 7), leaving a CWSS calculation, or removing the boron atoms within the first coordination sphere. Both manipulated calculations made it evident that the 40-eV peak is closely related to contributions from MS, i.e., any structural feature consisting of more than two atoms, as well as to boron atoms rather than to metal atoms. Deduced from CWSS results, the 28- and 50-eV peaks simply reflect the atomic distances and were largely unaffected by the computational manipulations. Evidently, the XANES feature around 40 eV stands for some additional information about the structure of the metallic glass.

### C. $\text{Fe}_{90}\text{Zr}_{10}$ (and $\text{Co}_{90}\text{Zr}_{10}$ )

XANES calculations were performed<sup>19</sup> in the same way as for the  $M_{80}\text{B}_{20}$  alloys ( $M$  = transition metal, Fe, or Ni) for both metal edges in  $\text{Fe}_{90}\text{Zr}_{10}$ , starting from four structural models for this alloy, three of which had been generated with an atomic-pair-potential relaxation

procedure<sup>20</sup> and agreed well with diffraction data. Due to negligible differences in the x-ray-diffraction data<sup>21</sup> between the Fe and the Co alloy, these models are also valid for  $\text{Co}_{90}\text{Zr}_{10}$ . One of the models, Brandt-Kizler No. 3 (BKN3) in Ref. 19, agreed well both with diffraction and XANES data for both edges. Similar to the case of the  $M_{80}\text{B}_{20}$  alloys, this peculiar model's Zr XANES spectrum exhibited a small hump, which vanished when MS was suppressed. For the Fe XANES in this case no spectral feature with an intimate relationship to MS processes could be found.

### III. PRESENT XANES INVESTIGATIONS

#### A. Samples

Samples of  $\text{Ni}_{80}\text{B}_{20}$  were produced in a thickness of 6  $\mu\text{m}$  by rf sputtering onto water-cooled Mylar foil. Samples of  $\text{Fe}_{80}\text{B}_{20}$  were produced by the planar flow cast method and purchased from Allied Signal Corp., Parsippany, NJ (U.S.A.), as Metglas 2605. The sample was thinned to its optimum thickness for x-ray absorption spectroscopy (XAS) measurements with a rf sputtering machine operated in the etching mode.  $\text{Co}_{90}\text{Zr}_{10}$  was prepared by melt spinning.  $\text{Fe}_{90}\text{Zr}_{10}$  was prepared by melt spinning by K. Pfahler, Max Planck Institut für Metallforschung—Institut für Physik, Stuttgart. The amorphous state of all samples was checked by x-ray diffraction, and for  $\text{Fe}_{90}\text{Zr}_{10}$  also by transmission-electron microscopy.<sup>22</sup> Crystalline  $\text{Fe}_2\text{Zr}$  was melted from the pure elements in an electron-beam furnace under high vacuum. This alloy is very brittle and cannot be rolled into a foil as a specimen for XAS measurements. Therefore, it was filed to a powder and stuck on several layers of adhesive tape in order to ensure sufficient thickness and homogeneity. The powder was also checked by x-ray diffraction for its proper structure and was found to be free of oxides. The samples were prepared during the author's Ph.D. work at the Max Planck Institut für Metallforschung—Institut für Werkstoffwissenschaft, Stuttgart.

#### B. X-ray-absorption measurements

X-ray-absorption measurements have been performed at the ROEMO II station at the Hamburger Synchrotronstrahlungslabor HASYLAB at Deutsches Elektronen-Synchrotron, DESY. The double-crystal monochromator was equipped with Si(311) crystals and exhibited an energy resolution of  $\Delta E < 1$  eV for the Fe and Ni edges and  $\Delta E \sim 4$  eV for the Zr edge. XANES data were extracted from the raw x-ray-absorption data by subtracting the monotonous background absorption applying the usual Victoreen fit. All samples and measurements have already been the object of previous studies, drawing less detailed conclusions.<sup>10, 13, 19</sup>

#### C. Brief description of the utilized structural models

##### 1. Model of Dubois, Gaskell, and Le Caër<sup>17</sup> for amorphous $\text{Ni}_{80}\text{B}_{20}$

This model assumed the short-range structure of  $\text{Ni}_3\text{B}$  (cementite structure) as the basic structural unit. Cen-

tered around the metalloid atom, the structural unit was left over as a trigonal prism. The three-dimensional space was filled with such small structural units that were dominantly linked via the crystallographic operation of chemical twinning. Structural domains with a range of size of 1 to 2 nm were assembled by this principle, and the intermediate space between such domains was also filled with such structural units, but obeying more complicated laws of construction. Finally, a structural relaxation using attractive Lennard-Jones potentials was performed. However, the structural units had already been almost in their energetic minimum;<sup>23</sup> therefore, this final relaxation procedure possibly induced smaller atomic displacements than is typical in the case of other modeling procedures. Out of several variations of this model, the presently used one is that related to Fig. 11(a) in Ref. 17.

##### 2. Model of Zweck<sup>18</sup> for amorphous $\text{Fe}_{80}\text{B}_{20}$

The construction of this model started with 1600 Fe and 400 B atoms, which were randomly distributed on a bcc lattice with a lattice constant of 0.3 nm. Next, the atoms were shifted from their positions by 0.09 nm in a random direction. Finally, a relaxation procedure was performed using strongly attractive pair potentials for the Fe-Fe and Fe-B pairs together with a weakly attractive one for the B-B pairs and under periodic boundary conditions. The potentials were of the Lennard-Jones-type and their values were chosen in agreement with literature data.

##### 3. Model BKN3 (Ref. 19) for amorphous $\text{Fe}_{90}\text{Zr}_{10}$

The first step of the procedure consisted in setting up a random arrangement of 150 Zr and 1350 Fe atoms within a cube. As the second step, a relaxation procedure was performed under the influence of repulsive pair potentials and under periodic boundary conditions. This procedure led to a rather homogeneous atomic distribution within the cube. Finally, attractive pair potentials were introduced and a consecutive relaxation loop procedure processed the arrangement to the final static model structure. The potentials were higher degree parabolas, similar to Morse potentials. Their depths, widths, and cutoff radii were different for the Fe-Fe, Fe-Zr, and Zr-Zr pairs, respectively.

#### D. Recent XANES calculations

In order to gain access to the peculiar reason for the shape of the XANES data, XANES calculations were resumed and extended to a much larger number of core atoms. For the  $M_{80}\text{B}_{20}$  alloy, only the models of Dubois *et al.* and Zweck were used because they had already provided the best agreement to the experimental XANES data.<sup>13</sup> In the case of the  $\text{Fe}_{90}\text{Zr}_{10}$  alloy, for the same reason only model BKN3 was used.<sup>19</sup> In pursuit of significant structural information, the number of selected core atoms and related XANES calculations was raised considerably to increase the statistical significance of the eventual result. The calculations were extended to a larger body of 322 metal core atoms taken from the total

number of 1475 metal atoms of the model of Dubois *et al.*, to 380 metal core atoms taken from 1600 metal atoms of the model Zweck, and to 60 Zr core atoms out of 150 Zr atoms in model BKN3, instead of only 40 in the earlier studies. The core atoms were selected such that the outward boundaries of the ensuing large clusters lay well within the perimeters of the model, because the XANES calculations require a sufficient cluster size to yield correct results, see, e.g., Refs. 9 and 12. This condition prevented the use of a larger number of core atoms. The same procedure as in Refs. 13 and 19 was followed, utilizing the identical scattering phase shifts as obtained by the MUF POT program and the same MS program.

#### IV. INTERPRETATION OF THE RESULTS FOR $\text{Ni}_{80}\text{B}_{20}$

The following discussions on the  $\text{Ni}_{80}\text{B}_{20}$  alloy also stand for  $\text{Fe}_{80}\text{B}_{20}$  and the use of Fe, Ni, or metal will be synonymous.

##### A. Explaining the 40 eV peak

In Fig. 1 the experimental data are compared to the calculated results for the Dubois and Zweck models, together with a random selection of many individually computed curves. The result of Fig. 1 obtained from 322 single results is practically identical to the previously published result from 40 single results.<sup>13</sup> Therefore, the convergence of the averaging is fast and the shape of the final result is already developed from only 20 single results (unpublished data). The variety of the single results demonstrates the large variation in curve shapes calling for interpretation. The results for  $\text{Fe}_3\text{B}$  in body-centered-tetragonal (bct) structure will be discussed in Sec. VI. Currently available programs to calculate XANES data are not capable of providing a direct path from a MS feature in a XANES curve to any triplet correlation. Even if there would be one, any neighbor atom is able to share different three-body correlations, which, at the same time, can increase or lower the absorption coefficient. Together with the considerable differences in atomic neighborhoods, when going from atom to atom, the chances to unravel such a complex process in a straightforward way do not seem very promising. Therefore, an indirect, statistical procedure was chosen as a first approach to the problem.

The 322 (Dubois) and 380 (Zweck) individual XANES results were visually sorted into several categories of curve shapes. To be discussed in the following for the model of Dubois and co-workers are 44 samples of curves with a very pronounced intermediate peak at the energy of 40 eV, hereafter termed Dubois-peak-strong-type (DPS), 57 curves with a weak peak, Dubois-peak-weak (DPW), 102 curves with a clear minimum at the same energy, Dubois-valley-strong (DVS) and 109 with a slightly softer minimum, Dubois-valley-weak (DVW). Finally, there were ten curves with irregular shapes fitting into none of these categories; they were omitted from further investigation. The averages of the types DPS, DPW, DVS, and DVW together with the average curve (DM) for the entire model are plotted in Fig. 2. Surprisingly,

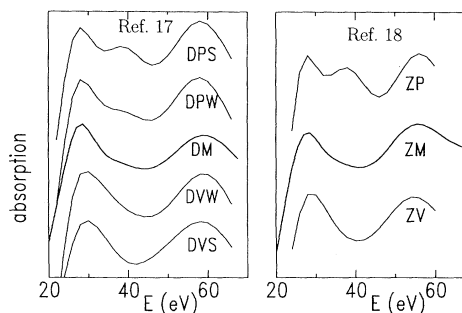


FIG. 2. Averages of peak and valley XANES results for the Dubois and Zweck models, together with the average for the whole model. The letters D, Z, P, V, M, S, and W stand for Dubois, Zweck, peak, valley, entire model, strong, and weak.

with the exception of the peak at  $40 \pm 2$  eV, no clear intermediate peaks at other energy positions could be observed. Therefore, the sum curves of the single DPS or DPW results again have a clear 40-eV peak.

The shapes of the results obtained for Zweck's model differed less than in the case of the Dubois model, and therefore were divided only into two categories of curves. Distinguished are 84 samples with a pronounced peak Zweck peak (ZP), and 133 samples with a clear minimum Zweck valley (ZV). There were 163 results with a less remarkable shape, in close similarity to the average for the entire model (ZM).

The subgroup of metal core central atoms belonging to the referenced results will also be named DPS atoms and analogously for the other types.

The calculations for the core atoms with the most pronounced shapes, DPS and DVS, were repeated with certain restrictions. The first restriction was to remove all boron atoms from the first coordination sphere around the core atoms (see Fig. 3). The original curve and the manipulated result are plotted in the same scale; therefore, for the DPS atoms a true reduction of the absorp-

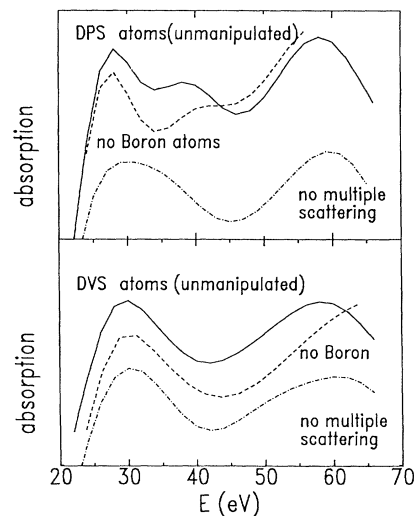


FIG. 3. XANES calculations with certain manipulations, applied to DPS- and DVS-type core atoms.

tion coefficient at the position of the 40-eV peak can be stated. A second restriction was to run the calculation with boron, but without MS, leaving a CWSS calculation. The curve belonging to the DPS atoms in Fig. 3 again demonstrates the fading of the interesting peak. The same manipulations applied to the calculations for the Strong-Valley core atoms led to no remarkable change in curve shapes (see lower part of Fig. 3.) The intimate relationship between the 40-eV peak and both the boron atoms and electron MS processes is obvious. The same manipulations cause the peak to also fade in the case of the Zweck model.<sup>13</sup>

### B. Examination of the radial density

From the coordinates of the models, the radial Ni-Ni and Ni-B number densities were calculated with a summation algorithm. The calculations were performed both for the core atom subsets and for the entire model. Small differences between the individual results showed up, but mainly for the metal-boron pairs and mainly beyond  $r = 0.35$  nm. However, if this small difference in Ni-B radial density should affect XANES simply by single back-scattering from the boron atoms, it should already appear in the case of CWSS calculations. The CWSS results in Fig. 3 demonstrate that this is not the case.

### C. Examination of triangles in the structure

A probable electron MS path is a triangular one back to the x-ray absorbing atom. The corners of the triangle, aside from the core atom, can consist either of two metal atoms or one metal and one boron atom.

#### 1. Examination of metal-metal-boron triangles

It is desirable to find a geometrical criterion, under which there is a strong contrast between the “peak” and “valley” core atoms. Significant differences between the neighborhoods of peak and valley core atoms could be found for triangles involving one metal and one boron neighbor atom. Surprisingly, it turned out that the distance to one of them had to be defined rather sharply, while the distance to the triangle’s other corner atom simply had to range within the first coordination sphere, below 0.32 nm.<sup>14,15</sup> It shall be anticipated that, despite this tolerance, the perimeters of the triangles of interest again are encountered as rather sharply defined.

The analysis was performed with a loop algorithm. For each selected core atom, pairs of neighbor atoms were selected, matching the desired range of bond lengths. For each couple of selected metal and boron neighbor atoms, the perimeter of the triangle was calculated, sorted with a stepwidth of 0.02 nm and counted per cell. Finally, the number of found triangles was divided by the number of core atoms engaged in the poll. The result is the number density of triangles in discrete steps of the cell width. The results can be displayed in the shape of a histogram whose barwidths represent the cells of 0.02 nm, the abscissas represent the perimeter of interest and the heights represent the average number of triangles

per metal core atom met in the referring perimeter cell width.

Figure 4 displays one set of results for defined triangles. The range of metal-boron radii was  $0.27 \text{ nm} < r < 0.28 \text{ nm}$ . The metal-metal distance of the second side was loosely limited to  $r < 0.32 \text{ nm}$ . More examples of such plots can be found in Ref. 10. There is a dramatic difference between the results for the DPS and DVS-type atoms as well as in the result for the whole model. For other ranges of metal-boron radii, these differences can disappear completely.<sup>10</sup> The results for the weak core atoms have been omitted from the figure to avoid confusion, but will be utilized again later. The first peak for a perimeter of approximately 0.72 nm corresponds to triangles with all atoms residing within the first coordination sphere and in more or less close vicinity. For perimeter values between 0.85 and 1.05 nm, the sides of the triangles opposite to the core atom have lengths between 0.4 and 0.5 nm, which means triangles with the two corner atoms almost at opposite sides of the core atom (bond angle  $\sim 120^\circ$ ). Such corner atom distances lie in the range of the second maximum in the partial pair-correlation function  $G_{\text{NiB}}$  (Refs. 14,15) suggesting three-body (or triplet) correlations to persist over even longer distances. Therefore, larger triangles were investigated with  $0.40 \text{ nm} < r_{\text{Ni-Ni}} < 0.48 \text{ nm}$  and  $0.26 \text{ nm} < r_{\text{Ni-B}} < 0.29 \text{ nm}$  (see Fig. 5). For the case of triangles with a perimeter of 1.3 nm, the results—always relying on the validity of the structural model—demonstrate that even correlations between peak core atoms and triplet correlations reaching into the second metal-metal coordination shell are likely. These triangles, due to their size, already match an aspect of medium-range order. The electron mean free path for low energies<sup>24</sup> is at its border to justify the consideration of even such long scattering paths.

The sum of the first peak in histograms like Fig. 4, more precisely only of triangles with atoms in close vicinity (only bond angles  $\sim 60^\circ$  equivalent to perimeters below  $\sim 0.8$  nm, but no bond angles  $\sim 120^\circ$  equivalent to perimeters above  $\sim 0.8$  nm), yields the number of trian-

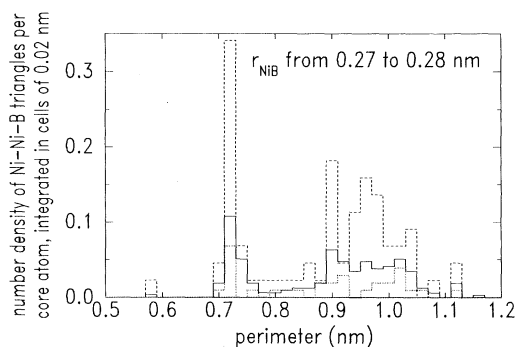


FIG. 4. Number density of Ni-Ni-B triangles per Ni core atom in the model of Dubois *et al.*, integrated in cells of 0.02 nm, dependent on the perimeter. Margins:  $0.27 \text{ nm} < r_{\text{Ni(core)-B}} < 0.28 \text{ nm}$ . Second side of triangle (Ni-Ni): confined to  $r < 0.33 \text{ nm}$ . Solid line: entire model; dashed line: DPS-type core atoms; dotted line: DVS-type core atoms.

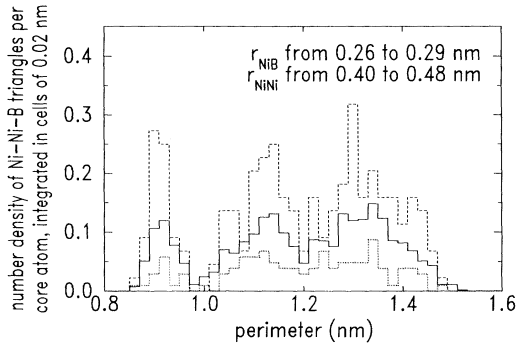


FIG. 5. Number density of Ni-Ni-B triangles per Ni core atom in the model of Dubois *et al.*, integrated in cells of 0.02 nm, dependent on the perimeter. Margins:  $0.26 \text{ nm} < r_{\text{Ni-B}} < 0.29 \text{ nm}$  and  $0.40 \text{ nm} < r_{\text{Ni-Ni}} < 0.48 \text{ nm}$ . Solid line: entire model; dashed line: DPS-type core atoms; dotted line: DVS-type core atoms. This diagram visualizes triplet correlations including core atom and atoms in the first- and second-neighbor shells.

gles counted for the referring side length, disregarding the value of the perimeter of the triangles, which, however, varies only to a minor degree.

Such sums in their dependence on the metal-boron side length are displayed in the upper part of Fig. 6, separately for the entire models, the peak and valley subsets, and also for both the Dubois and Zweck models.

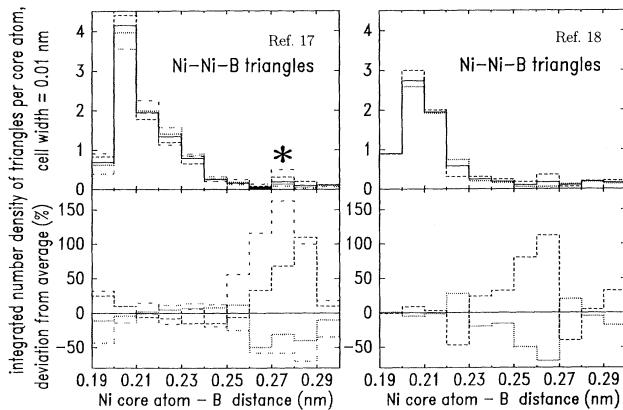


FIG. 6. Number densities of Ni-Ni-B triangles per Ni core atom integrated in cells of 0.01 nm from the first maxima (perimeters  $< 0.8 \text{ nm}$ ) of number density integrals as in Fig. 4, dependent on the Ni<sub>core</sub> - B distance. Included are data for the peak and valley atomic subsets and for the entire model. Left part: results for the Dubois model; right part: for the Zweck model. Top section: total numbers; bottom section: deviation from average expressed as percentage. Full lines: entire model; dashed line: peak core atoms, strong and weak merged; dotted line: valley core atoms, strong and weak merged. Spaced line (dashed or dotted): only strong subsets. A practical example: for the Dubois model, the DPS value of 0.5 for a Ni-B distance of 0.275 nm, marked with an asterisk, equals the main DPS bar in Fig. 4, plus its neighbor bars up to a perimeter of 0.8 nm. Note that for other radii the peaks as in Fig. 4 are less sharp, see, e.g., Ref. 10.

The numerical values of these sums become persuasive regarding the link to the structure. The partial coordination numbers  $N$  (metal-metal) and  $N$  (metal-boron) in the alloy amount to ten and two, respectively. Therefore, each core atom is surrounded by  $2 \times 10 = 20$  metal-metal-boron triangles. Only configurations with bond angles around  $60^\circ$ , but not around  $120^\circ$  shall be discussed; therefore, half of the 20 have to be omitted, leaving approximately 10 triangles. This number equals the sum of all data points in the upper left part of Fig. 6 which again amounts to approximately 10.

In the lower part of Fig. 6, the deviations from the model's average number are expressed as percentage. In the case of the Dubois model both the strong peak or valley results are shown as well as the merged strong and weak results. The strong results yield rather extreme values pointing clearly to the structural features of interest. On the other hand, the strong and weak results are less noisy due to the larger number of core atoms and counted triangles. Since the way of sorting the individual results into strong and weak categories was a bit arbitrary, the united strong and weak results altogether are more reliable.

The results obtained for the Zweck model generally repeat the trend as observed for the Dubois model, although the two models have been constructed by different principles. This shows that the overall trend of the left- and right-hand sides of Fig. 6 is not simply a chance result but instead seems to be a structural feature independent of the way of model building. In the case of the Zweck model, the trend for the very short metal-boron distances appears relatively poor, because Zweck's modeling algorithm was less successful in achieving the closest possible atomic distances. Therefore, for this model the pair-correlation functions agreed less well with the experimental data than those of the model of Dubois *et al.*<sup>16</sup> But these minor differences are still within the frame of general agreement between the two models and their triangle frequencies.

The number of triangles in the range where the peak and valley atoms exhibit interesting differences is rather small and, therefore, gives rise to suspicions about statistical uncertainties. For instance, for the Dubois model, the number of total Ni-Ni-B triangles at  $r_{\text{Ni-B}} = 0.275 \pm 0.005 \text{ nm}$  (see asterisk in Fig. 6) equals the ordinate value times the total number of core atoms which is 22 for the 44 DPS core atoms. For the 101 DPS and DPW core atoms, this number amounts to 35 versus only 26 around the 211 DVS and DVW core atoms and versus 61 triangles for all 312 core atoms in the model (excluding ten queer core atoms, see Sec. IV A). Statistical fluctuations amounting to even ten seem to be possible within the confidence level. However, taking into account not only one single histogram bin but the whole range of triangles with measures above the average, i.e.,  $0.25 \text{ nm} < r_{\text{Ni-B}} < 0.30 \text{ nm}$ , there is a total amount of 53 triangles for the 44 DPS and 97 triangles for the 101 DPS and DPW case versus 83 triangles for the 210 (DVS and DVW) core atoms. For the small triangles with  $0.19 \text{ nm} < r_{\text{Ni-B}} < 0.21 \text{ nm}$ , the overall numbers amount to 240 for DPS, 545 for DPS and DPW, 401 for DVS, and 960

for DVS and DVW. Remember the larger number of valley atoms versus peak atoms. For the larger triangles, the total numbers are still too small to use the diagram as a kind of precise inventory of the structural elements, but they are large enough to leave no doubt on the trend as described. In the case of the Zweck model, the corresponding numbers would have similar amounts.

Triplet correlations as revealed by these statistics should now be a challenge to the theory of glass formation to study the role of these particular structural elements.

The smallest triangles (see left limit values in Fig. 6) are simply formed of metal and boron atoms, tightly pressed together.

For metal-boron distances of  $0.235 \pm 0.015$  nm for the Zweck model around 0.225 nm, the peak atoms are very weakly deficient in triangles. This bond length agrees, for instance, approximately with the distance between the B atom in the center of a trigonal prism and a Ni cusp atom capping a square face of the prism.<sup>25</sup>

The metal-boron distance of  $0.275 \pm 0.015$  nm as in Fig. 4 is more difficult to understand. The value is much larger than the average Ni-B distance in the amorphous alloy and still larger than the mentioned Ni cusp atom-boron distance.

## 2. Examination of metal-metal-metal triangles

The same procedure as above has also been applied to triangles consisting only of metal atoms (see Fig. 7). For direct comparison the percentage scale is identical to the one in Fig. 6. The absolute numbers (see top sections of Fig. 6) are larger than for the metal-metal-boron case; therefore, possible statistical noise does not deserve atten-

tion. Also for metal triangles there is some contrast between peak and valley atoms regarding triangles with one side of approximately 0.29 nm, but the contrast is much weaker than in the case of the metal-metal-boron triangles. Therefore, the metal-metal-boron triangles play a more important role for the differences in peak and valley results.

## 3. Lengths of the other sides of the triangles

The importance of one side of the triangle has been discussed, but not the lengths of the other two sides. It is difficult to figure out a description to visualize lengths of all three sides simultaneously and clearly. An interesting attempt to visualize triplet correlations has been tried by Filipponi *et al.*,<sup>26</sup> who represented side lengths and the bond angle at the core atom for a structural model for amorphous Si by a cloud of dots in a Cartesian diagram. However, even in this representation it is difficult to unambiguously retrieve information on the other sides of the triangle. In addition, a portioning of the results into different triangle side lengths would most probably raise statistical noise and, therefore, become confusing rather than elucidating. Instead, a closer study of the perimeters can reveal some additional information.

The peak values of the perimeters of Ni-Ni-B triangles (as in Fig. 4), minus the length of the defined side, results in values between 0.465 nm (for Ni-B distances between 0.19 and 0.20 nm) and 0.445 nm (for Ni-B side length between 0.29 and 0.30 nm), almost identical for both the Dubois and Zweck models. The other side of the triangle consists of another Ni-B bond, shorter than a Ni-Ni bond. Therefore, even if the defined side length deviates considerably from the average values, the other distances still remain in the range of close contact, well within the peaks of the partial pair-correlation functions. If, for instance, the remaining rest of the perimeter should not be divided evenly among the two bonds (in other words, if one of the bonds would have the smallest ever possible value instead of an average one see the partial pair-correlation functions<sup>14,15</sup>)—this would result in a change of the bond angle of the core atom's site of not more than 5°, i.e., the shape of the triangle is not essentially changed. Therefore, variations of the two other bond lengths in the possible range do not lead to significant different shapes of the triangle. To extend the description of the investigated triangles in more detail would not reveal additional knowledge.

## 4. Would bond angles describe the structural features better?

Bond angles have been suggested as a measure to describe triplet correlations in amorphous materials.<sup>27</sup> The bond angles at the core atoms site have been calculated for cases as in Fig. 4, with  $r_{\text{Ni-B}}$  varying between 0.19 and 0.28 nm. Provided that the remaining perimeter of the triangle, minus the defined side length, is the sum of average Ni-B and Ni-Ni distances (see diffraction data), the angles vary only between 53° and 45°, respectively. Yet these angles are subject to variations by  $\sim \pm 5^\circ$  around

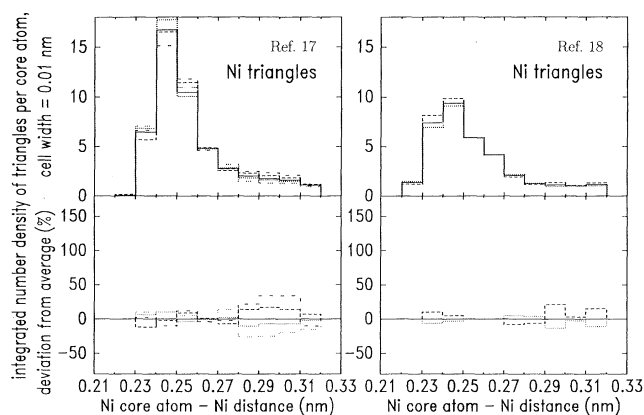


FIG. 7. Number densities of Ni-Ni-Ni triangles per Ni core atom integrated in cells of 0.01 nm from the first maxima (perimeters  $< 0.8$  nm) of number density integrals analogous to Fig. 4, dependent on one  $\text{Ni}_{\text{core}} - \text{Ni}$  distance. Included are data for the peak and valley atomic subsets and for the entire model. Left part: results for the Dubois model; right part: for the Zweck model. Top section: total numbers; bottom section: deviation from average expressed as percentage. Full lines: entire model; dashed line: peak core atoms, strong and weak merged; dotted line: valley core atoms, strong and weak merged. Spaced line (dashed or dotted): only strong subsets.

these values, due to possible variations of the remaining two bonds (see Sec. IV C 3). Therefore, a description of the examined triangles in terms of bond angle does not seem to resolve their shapes more clearly. The present graphical representation seems to be better tailored to the electron multiple-scattering process because different triangles with different bond angles can have the same perimeter.

#### 5. On the impact of the metal-metal-boron multiple-scattering processes

The results of Sec. IV C 2 (Fig. 6) enable one to discern between triangles with core atom–boron distances of (i) 0.19 to 0.21 nm, (ii) 0.21 to 0.26 nm, and (iii) 0.26 to 0.29 nm. The short-range order around the DPS atoms has a slight surplus of the first- and the third-mentioned measure. The partial coordination numbers  $N(\text{metal-boron})$  as integrated only within the corresponding ranges amount to 1.3, 0.8, and 0.3, respectively. It should be noted that core atom–boron distances of 0.26 to 0.29 nm, which were found to provide such a distinguishing feature between peak and valley atoms (see Fig. 4) show up for only a third of the DPS core atoms (as well as for the DPW atoms).

As discussed in Sec. IV A, XANES calculations for the DPS atoms after removing all boron atoms from the first coordination sphere (see Fig. 3) have demonstrated the importance of the boron atoms for the existence of the 40-eV peak. In addition, XANES calculations have been repeated after removing only the boron atoms the range between 0.19 and 0.21 nm and between 0.26 and 0.29 nm (see Fig. 8). Obviously these boron atoms play a very important role for the existence of the 40-eV peak, but not with an overwhelming impact. It must be noted that the electron-scattering power of boron is known to be small for the EXAFS region but becomes quite strong for the low  $k$  values as in XANES.<sup>28</sup>

Taking into account this result together with the small number of boron atoms in the range between 0.26 and 0.29 nm the following conclusions may be drawn.

It was evident that the short-range order of core atoms with the 40-eV peak is likely to have a surplus of triangles with selected metal-boron distances. Nevertheless, due to

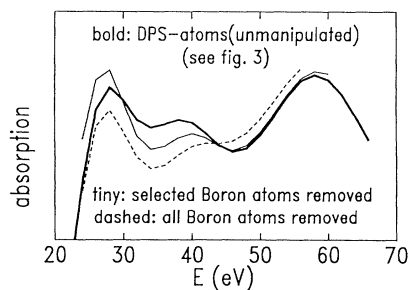


FIG. 8. XANES calculations for DPS core atoms with certain manipulations: calculations after removing all boron atoms from the first coordination sphere, after removing only boron atoms with  $0.19 \text{ nm} < r_{\text{Ni-B}} < 0.20 \text{ nm}$  and  $0.26 \text{ nm} < r_{\text{Ni-B}} < 0.29 \text{ nm}$ , and without removing boron atoms.

their limited number, these triangles are not necessarily the one and only cause of this peak. We have already recognized statistical evidence of a surplus of triangles reaching into the second coordination sphere (Fig. 5). Moreover, there are possible quadruple scattering paths including the absorber atom and (i) only one neighbor atom,<sup>26</sup> (ii) two neighbor atoms,<sup>26</sup> or (iii) three neighbor atoms, thereby introducing a four-body correlation. Therefore, the described phenomenon in the first coordination sphere shows up parallel to other, more hidden, structural features, and may be higher than triplet correlation, which may be linked to the described ones due to geometrical constraints of the dense filling of space and can cooperate to yield the final scattering result. The discussion of triangles within the first coordination sphere, therefore, should be regarded as a preliminary insight into the problem. In the present work it was, however, not possible to find more correlations with such pronounced contrast for the peak and valley atoms like the one shown in Fig. 6.

#### 6. On the importance of the described metal-metal-boron triangles for the description of the structure

Although the mentioned triangles have been shown to play an important role in understanding the shape of the XANES data, nevertheless they form a minority among all occurring triangles. Therefore, it is questionable if they are at all worthy of attention or if a structural description of the metallic glass should center on the majority of triangles with average measures. The answer may depend on the attitude of the researcher: “Those, whom I would like to name ‘universalists’ are convinced of and imagine, despite vast deviations and varieties, that a general character exists everywhere and may possibly be discovered. The others, whom I want to name ‘singularists’, in general, admit this principle, and even more so, they observe, determine, and teach accordingly. However, they are always alert to discover exceptions, where the character has not totally evolved, and in that they are right. Their mistake, however, is to misconceive the fundamental where it is veiled and to deny it when it is hidden. Since both conceptions are original and will forever stand opposite without merging or neutralizing, one must abstain from dispute and express one’s opinion clearly and plainly.”<sup>29</sup>

While diffraction and other methods of structural determination describe structures mainly in an averaged way, i.e., under universalists aspects, the present study introduces singularists’ information focusing attention on a minority of deviating structural elements.

Perhaps the role of this minority of structural elements is similar to the one of structural modifiers in the case of mineral glasses. In each case, any structural model for these metallic glasses lacking such triangles would surely be not bad but imperfect.

## V. INTERPRETATION OF THE RESULTS FOR Fe<sub>90</sub>Zr<sub>10</sub>

As mentioned already in Sec. II C, the calculated results for the Zr edge contain a small hump feature, which

appeared best (although weak) in the case of model BKN3 and which vanished when MS was excluded. In Fig. 9 the experimental Zr XANES data for the amorphous  $\text{Fe}_{90}\text{Zr}_{10}$  and  $\text{Co}_{90}\text{Zr}_{10}$  alloys and for crystalline  $\text{Fe}_2\text{Zr}$  are compared to the computed result for model BKN3. Since for the Fe XANES data no particular structural feature depending on MS processes could be discovered,<sup>19</sup> only the Zr XANES data will be discussed in the following.

### A. Explaining the 40 eV peak

Analogous to the results for  $\text{Ni}_{80}\text{B}_{20}$ , in the case of Zr, the 60 individual XANES results could be sorted into 16 results with a pronounced peak (termed ZFP in the following, for Zr-Fe-Peak), 21 results with a clear valley outline (ZFV) and 23 ones with an indifferent shape, more or less identical to the average for the whole model (ZRM), are averaged as seen in Fig. 10. Included in the diagram are the results for CWSS calculations, as dotted lines. Similar to the examples in Fig. 3, in this case the peak curves contain the strongest MS contribution, suggesting some higher-order correlation to be responsible for the shape.

### B. Examination of Zr-Fe-Fe triangles

Similar to  $\text{Ni}_{80}\text{B}_{20}$ , no remarkable contrast in the radial densities around the peak and valley core atoms could be found. Since the 40-eV peak again is linked to multiple-scattering processes,<sup>19</sup> the abundance of Zr-Fe-Fe triangles around Zr core atoms has been investigated in the same spirit as in Sec. IV C 2. Further figures analogous to Fig. 4 are not included in the present paper because

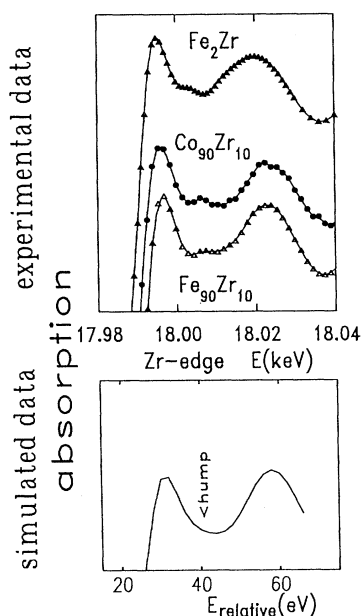


FIG. 9. Top: experimental Zr XANES data for crystalline and amorphous (Fe, Co)-Zr alloys and for crystalline  $\text{Fe}_2\text{Zr}$ . Bottom: calculated XANES curve for model BKN3 (see Ref. 19).

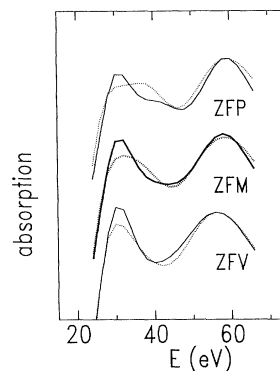


FIG. 10. Averages of calculated peak and valley curves and the entire model BKN3 together with CWSS results, included as dotted lines.

they would not have been essentially different. Equivalent to Fig. 6, in Fig. 11 the sums of numbers of triangles encountered for defined Zr neighbor distances are shown. The lower part of Fig. 11 again expresses the deviation from the average number as percentage and in the same scale as for the  $\text{Ni}_{80}\text{B}_{20}$  case, for comparison. For this alloy, one obtains a significant correlation between peak core atoms and triangles with measures above the average, i.e., one side length between 0.28 and 0.31 nm, however, with the sign opposite to the trend for the  $\text{M}_{80}\text{B}_{20}$  alloys. The peak XANES outline is correlated to a reduced number of triangles of the above-mentioned measure.

Due to the small number of Zr atoms in the model and the corresponding smaller number of calculational results, Fig. 10 is buried with some statistical uncertainty.

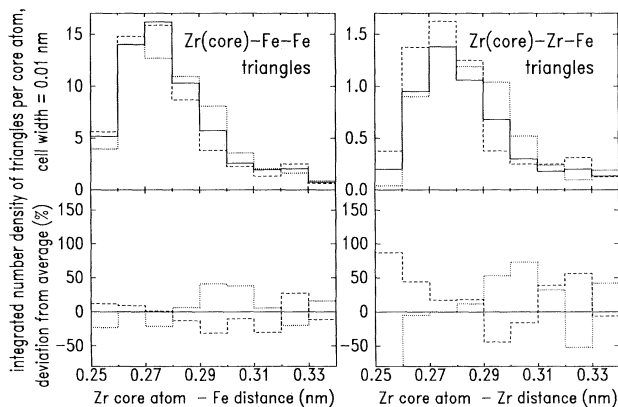


FIG. 11. Number densities of Zr-Fe-Fe triangles per Zr core atom integrated in cells of 0.01 nm from the first maxima (perimeters  $< 0.8$  nm) of number density integrals analogous to Fig. 4, dependent on one  $\text{Zr}_{\text{core}}-\text{Fe}$  distance. Left part: data for Zr-Fe-Fe triangles in model BKN3 for the peak and valley atomic subsets and for the entire model. Right part: data for Zr-Fe-Zr triangles in model BKN3, for the peak and valley atomic subsets and for the entire model. Top section: total numbers; bottom section: deviation from the average, expressed as percentage.

It is partly compensated by the larger number of triangles counted around the small number of core atoms. For instance, for  $0.29 \text{ nm} < r_{\text{Zr-Fe}} < 0.32 \text{ nm}$ , the total number of Zr-Fe-Fe triangles amounts to 281, 116, and 604 for the 21 valley, the 16 peak core atoms, and the 60 core atoms of the entire model, respectively. Therefore, the trend in Fig. 10 is reliable but not very precise.

Equivalent to Fig. 5, correlations between Zr core atoms, Fe in the first and Fe in the second coordination sphere have been investigated (see Fig. 12). Also for this triplet correlation reaching beyond the first shell, the peak atoms suggest a diminished correlation over longer distances.

### C. Examination of Zr-Zr-Fe triangles

Analogous to Sec. VB, Zr-Zr-Fe triangles have been examined. The results for the evaluation of these triangles are contained in the right part of Fig. 11. They have to be regarded with great care to the small and uncertain number of Zr atoms in the first-neighbor shell. Tentatively assuming validity of model BKN3, also for the Zr-Zr correlation, the results confirm the same trend for Zr-Zr-Fe triangles, similar to the Zr-Fe-Fe ones in the left part of Fig. 11.

## VI. SIMILARITY TO XANES CURVES OF CRYSTALLINE COMPOUNDS

The similarity between short-range order in metallic glasses and crystalline reference alloys has often been stressed (see, e.g., Ref. 30). In the case of  $\text{Fe}_{80}\text{B}_{20}$ ,  $\text{Fe}_3\text{B}$  in bct structure,<sup>31</sup> admittedly highly distorted, was claimed to represent the short-range order in the amorphous alloy. Since  $\text{Fe}_3\text{B}$  is metastable, only a calculated XANES curve (Fig. 1) is available. Some similarity to the experimental data can be stated, however, the hump's energy position is wrong.

$\text{Fe}_2\text{Zr}$  in cubic  $\text{Cu}_2\text{Mg}$  structure<sup>31</sup> is not the alloy with the stoichiometry closest to  $\text{Fe}_{90}\text{Zr}_{10}$ . However, pure

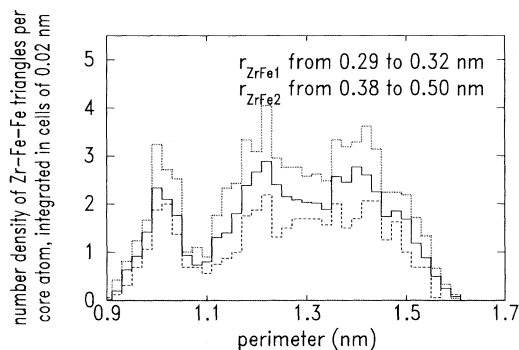


FIG. 12. Number density of Zr-Fe-Fe triangles per Zr core atom in model BKN3 integrated in cells of 0.02 nm, dependent on the perimeter. Margins:  $0.29 \text{ nm} < r_{\text{Zr(core)-Fe(1)}} < 0.32 \text{ nm}$  and  $0.38 \text{ nm} < r_{\text{Zr(core)-Fe(2)}} < 0.50 \text{ nm}$ . Solid line: entire model; dashed line: ZFP-type core atoms; dotted line: ZFV-type core atoms. This diagram visualizes triplet correlations including core atom and atoms in the first- and second-neighbor shells.

phases of  $\text{Fe}_3\text{Zr}$  or  $\text{Fe}_{23}\text{Zr}_6$ , which have a more similar stoichiometry, are very difficult to prepare.

For both cases,  $\text{Fe}_3\text{B}$  and  $\text{Fe}_2\text{Zr}$ , a certain similarity between crystalline and amorphous data cannot be denied. On the other hand, we have seen in Sec. IV and V how XANES calculations based on structural models are able to nicely reproduce experimental data without assuming any crystalline (like) short-range order. Radial distribution functions and triangle shapes in the crystalline reference compounds differ considerably from the data for the structural models as well as from the outstanding values for the peak core atoms. Therefore, this is an instructive example for a tempting similarity in XANES shapes, which can lead to premature conclusions. In the author's opinion, to discuss XANES curves as fingerprints of a certain short-range geometry in the present cases is not justified. The success of the calculation from amorphous models demonstrates that there is no need to assume *ab initio* crystallinelike short-range order to interpret XANES data. However, due to this ambiguity, a successful XANES calculation from a conceptually different structural model cannot be excluded for the future. Such a model, however, would have to agree simultaneously both with diffraction and XANES data as well as with macroscopic density and other solid-state properties. Altogether, this seems to be very difficult.

## VII. CONCLUSIONS

In the present study, XANES spectra of metallic glasses have been interpreted in great detail. It demonstrates that XANES simulation can be very useful in investigating triplet correlations in structures of noncrystalline materials and that similarities between the XANES shapes of amorphous alloys and similar crystalline counterparts can be superficial and must be regarded with caution.

Since the present study could not rely upon any generally approved scheme, new approaches to data interpretation and structural description had to be taken. Triangles with one well-defined side turned out to provide a significant link between structural properties and typical shapes of calculated XANES curves, because triangles are well tailored to the electron multiple-scattering processes.

For the case of the metallic glasses  $\text{Ni}_{80}\text{B}_{20}$  and  $\text{Fe}_{80}\text{B}_{20}$ , the reason for the good XANES simulation from the models of Dubois *et al.* and Zweck could be traced to metal-metal-boron triangles of well-defined sizes. The smallest ones are atoms within the closest possible distances. Other ones, with metal-boron lengths of 0.26 to 0.29 nm, demonstrate the importance of structural elements, which have so far attracted little attention as structural building blocks in the theory of glass formation. For  $\text{Fe}_{90}\text{Zr}_{10}$  and  $\text{Co}_{90}\text{Zr}_{10}$ , the results point to the importance of structural elements with a lesser variance than in the ones derived from the proposed structural model.

In both cases, the  $M_{80}\text{B}_{20}$  and the  $M_{90}\text{Zr}_{10}$  alloys, the outline of the experimental XANES curves is more sharply pronounced than the calculated results. As the

computer code used perfectly reproduces sharp XANES features for crystalline materials (cf. Ref. 12), the difference cannot result from weaknesses of the theory.

Rather, if the structural models could be modified to incorporate a larger fraction of structural elements like the peak core atoms, this could certainly improve the agreement between theory and experiment.

The recognized importance of structural elements with measures different from the average may stimulate enough interest to perform high- $Q$  high-resolution diffraction and EXAFS experiments not only from the point of view of mean atomic distances but also respecting the shape of the pair distribution functions<sup>32</sup> and their values aside the peak top.

- <sup>1</sup>Proceedings of the Workshop on Investigation of Higher Order Correlation Functions Grenoble, 1985, edited by J. B. Suck, D. Quitmann, and B. Maier [J. Phys. (Paris), Colloq. **46**, C9 (1985)].
- <sup>2</sup>P. A. Egelstaff, *An Introduction to the Liquid State* (Academic, London, 1967).
- <sup>3</sup>For example, T. Fujiwara and Y. Ishii, J. Phys. F **10**, 1901 (1980); F. Lançon, L. Billard, and A. Chamberod, *ibid.* **14**, 579 (1984); G. Bushnell-Wye, J. L. Finney, and J. F. Quinn, in *Proceedings of the Fourth International Conference on Rapidly Quenched Metals (RQ4), Sendai, Japan, 1981*, edited by T. Masumoto and K. Suzuki (Japan Institute of Metals, Tokyo, 1982), p. 271; B. J. Gellatly and J. L. Finney, *ibid.*, p. 275.
- <sup>4</sup>J. U. Madsen and R. M. J. Cotterill, in *Liquid and Amorphous Metals*, edited by E. Lüscher and H. Coufal (Sijthoff and Noordhoff, Alphen aan den Rijn, The Netherlands, 1980).
- <sup>5</sup>P. J. Durham, J. B. Pendry, and C. H. Hodges, Solid State Commun. **38**, 159 (1981).
- <sup>6</sup>P. J. Durham, J. B. Pendry, and C. H. Hodges, Comput. Phys. Commun. **25**, 193 (1982).
- <sup>7</sup>D. D. Vvedensky, D. K. Saldin, and J. B. Pendry, Comput. Phys. Commun. **40**, 421 (1986).
- <sup>8</sup>J. E. Müller, O. Jepsen, O. K. Andersen, and J. W. Wilkins, Phys. Rev. Lett. **40**, 720 (1978); J. E. Müller and J. W. Wilkins, Phys. Rev. B **29**, 4331 (1984).
- <sup>9</sup>P. Kizler and S. Steeb, in *Proceedings of the Fifth XAFS Conference, Seattle, WA, 1988*, edited by J. M. de Léon *et al.* [Physica **158B**, 392 (1989)].
- <sup>10</sup>P. Kizler, Phys. Rev. Lett. **67**, 3555 (1991).
- <sup>11</sup>P. H. Gaskell, D. M. Glover, A. K. Livesey, P. J. Durham, and G. N. Greaves, J. Phys. C **15**, L597 (1982).
- <sup>12</sup>G. N. Greaves, P. J. Durham, G. Diakun, and P. Quinn, Nature (London) **294**, 139 (1981); P. Kizler, Phys. Rev. B **46**, 10 540 (1992).
- <sup>13</sup>P. Kizler, P. Lamparter, and S. Steeb, Z. Naturforsch. **44a**, 189 (1989).
- <sup>14</sup>E. Nold, P. Lamparter, H. Olbrich, G. Rainer-Harbach, and S. Steeb, Z. Naturforsch. **36a**, 1032 (1981).
- <sup>15</sup>P. Lamparter, W. Sperl, S. Steeb, and J. Blétry, Z. Naturforsch. **37a**, 1223 (1982).
- <sup>16</sup>P. Kizler, P. Lamparter, and S. Steeb, Z. Naturforsch. **43a**, 1047 (1988); P. Kizler, Ph.D. thesis, University of Stuttgart, Germany, 1988.
- <sup>17</sup>J. M. Dubois, P. H. Gaskell, and G. Le Caër, Proc. R. Soc. London Ser. A **402**, 323 (1985).
- <sup>18</sup>U. Krey, H. Ostermeier, and J. Zweck, Phys. Status Solidi B **144**, 203 (1987). J. Zweck, Ph.D. thesis, University of Regensburg, Germany, 1987.
- <sup>19</sup>P. Kizler, P. Lamparter, and S. Steeb, Z. Naturforsch. **44a**, 7 (1989).
- <sup>20</sup>E. H. Brandt and H. Kronmüller, J. Phys. F **17**, 1291 (1987).
- <sup>21</sup>H. S. Chen, K. T. Aust, and Y. Waseda, J. Non-Cryst. Solids **46**, 307 (1981).
- <sup>22</sup>K. Pfahler, Ph.D. thesis, University of Stuttgart, Germany, 1987.
- <sup>23</sup>J. M. Dubois (private communication).
- <sup>24</sup>B. K. Teo, *EXAFS: Basic Principles and Data Analysis* (Springer, Berlin, 1986), p. 92.
- <sup>25</sup>See, e.g., Fig. 10 and related discussion in Ref. 15.
- <sup>26</sup>A. Filipponi, A. Di Cicco, M. Benfatto, and C. R. Natoli, Europhys. Lett. **13**, 319 (1990).
- <sup>27</sup>See, e.g., J. Hafner, J. Phys. F **12**, L205 (1982); also Refs. 1 and 2.
- <sup>28</sup>B. K. Teo and P. A. Lee, J. Am. Chem. Soc. **101**, 2815 (1979); A. G. McKale, B. W. Veal, A. P. Paulikas, S. K. Chan, and G. S. Knapp, *ibid.* **110**, 3763 (1988); Fig. 1 in P. Kizler, Phys. Rev. B **47**, 5662 (1993).
- <sup>29</sup>J. W. Goethe, No. 229, *Sprüche in Prosa (Aphoristic Prose)*, from *Naturwissenschaftliche Schriften (Works on Natural Science)*, edited by R. Steiner (Kürschner's Deutsche National Literatur, Stuttgart, 1883), Vol. 2 (recent edition published by Freies Geistesleben, Stuttgart 1967).
- <sup>30</sup>See, e.g., H. Hermann and N. Mattern, J. Phys. F **16**, 131 (1986); J. L. Walter, S. F. Bartram, and I. Mella, Mater. Sci. Eng. **36**, 193 (1978); I. Vincze, T. Kemeny, and S. Arajs, Phys. Rev. B **21**, 937 (1980); E. Zschech, W. Blau, V. K. Fjodorov, and M. A. Sheromov, Nucl. Instrum. Methods **282**, 586 (1989).
- <sup>31</sup>W. B. Pearson, *Handbook of Lattice Spacings and Structures of Metals and Alloys* (Pergamon, Oxford, 1967).
- <sup>32</sup>P. Kizler, J. Non-Cryst. Solids **162**, 144 (1993).